

Efficient mathematical representations for computing the forced wave dynamics of anisotropic laminated composites

Evgeny Glushkov · Natalia Glushkova ·
Artem Eremin

Received: date / Accepted: date

Abstract Explicit integral and asymptotic representations for the total wave fields and specific guided waves generated in anisotropic laminate structures by surface loads are offered as a basis for low-cost computer models. Their abilities are demonstrated and experimentally verified with two practically important examples: a reconstruction of effective elastic moduli of a fiber-reinforced composite plate and a frequency tuning of a patch piezoactuator with accounting for the radiation directivity caused by the plate's anisotropy.

Keywords Anisotropic composites · Integral approach · Guided wave asymptotics · Identification of material properties · Frequency tuning

1 Introduction

Nowadays composite materials become widespread in engineering applications, first of all, in aerospace, power and chemical industry. Structural elements produced from the composites possess more complicate mechanical properties than components manufactured from isotropic materials, e.g., from aluminium alloys. Therefore, computer simulation of their elastodynamic behavior is a much more challenging task.

In engineering design practice, the difficulties relating to complex geometry and material properties are commonly overcome by the use of finite element (FEM) or finite difference (FDM) methods that are based on a mesh discretization of structural components. These and related methods are implemented in various commercial packages and, due to their indisputable advantages, they are considered as universal tools of computer simulation. However, a discretization of lengthy structures for wave propagation problems, which requires more and more elements as distances or frequencies increase, becomes time and, especially, memory consuming. Therefore, efficient alternatives to these approaches allowing significant reduction of computation costs have been recently developed and successfully

E. Glushkov, N. Glushkova, A. Eremin
Kuban State University,
Institute for Mathematics, Mechanics and Informatics,
Stavropolskaya 149, 350040, Krasnodar, Russia
Tel.: +7-861-2199-517
Fax: +7-861-2199-502
E-mail: evg@math.kubsu.ru

implemented for layered composite dynamics. For instance, these are the spectral element method (SEM) [19, 24], which is a high-order FEM, and the local interaction-simulation approach (LISA) [16]. Another promising approach adjusted to waveguides with plane-parallel boundaries is the spectral finite element method (SFEM) [11], which combines integral Fourier transforms for time and spatial in-plane variables and the Rayleigh-Ritz method with the transverse coordinate.

With domains of simpler, classical form, e.g., for laminate plates with local inhomogeneities, analytically-based methods are also suitable. Explicit analytical representations for guided waves (GWs) do not require any spatial discretization, and so they remain practically costless irrespective of the sample's size. Therefore, hybrid schemes, combining mesh or boundary-element discretization of local areas (flaws, stringers, rivets, etc.) with an analytically-based continuation of incident and scattered wave fields among them, are of great interest, as well.

Besides the designing purposes, the mathematical modeling is an indispensable part of GW structural health monitoring (SHM) [6, 20]. The SHM aims at diagnosis and failure prevention of vitally important components. It is based on the GW property to propagate in plate-like structures for long distances exhibiting high sensitivity to local inhomogeneities of any kind including hidden defects such as cracks, delaminations, and surface-breaking fractures. The defects manifest themselves in scattered GWs, which also propagate for long distances and may be registered by sensors. The incident and diffracted GWs are actuated and sensed by piezoelectric wafer active sensors (PWAS) attached to or incorporated into the inspected structure. In this way PWAS arrays control large areas of structural components. The location of defects is determined by the arriving time of reflected signals (time-of-flight – TOF), while the patterns of scattered diagrams provides information about defects' properties.

The mathematical modeling is used here for the prediction of velocities and radiation diagrams of GWs actuated in specific structures by driving signals of prescribed shapes and central frequencies, as well as for the scattered wave field simulation. With isotropic plates, the GWs are well-studied Lamb waves. Their modal characteristics are independent of the direction of wave propagation over the plate, while they become directionally dependent in anisotropic composite structures. The latter essentially complicates the mathematical modeling. Nevertheless, analytically-based methods of wave analysis in anisotropic laminate structures have been also well developed [18, 22, 23]. The GWs have been derived and used here in the form of plane waves (2D normal modes). Such expressions yield a good insight into the peculiarities of GW propagation in anisotropic structures, however, they are ill-suited to the approximation of cylindrical waves, spreading out from local sources and obstacles. The cylindrical GWs are of prime concern for a 3D wave analysis in composite plates, therefore, a derivation of their closed asymptotic representations strictly accounting for the angular dependency of characteristics induced by the material anisotropy has been an urgent problem.

In a 2D statement, it is possible to represent the wave field generated by a local source in terms of a one-fold path integral in the wavenumber domain. The residues from the real poles ζ_n of its integrand yield close analytical representations for the plane GWs generated by the source, e.g., for the waves propagating in the x direction, in the form

$$\mathbf{u}_n(x, z) = t_n \mathbf{a}_n(z) e^{i(\zeta_n x - \omega t)}, \quad n = 1, 2, \dots \quad (1)$$

The amplitude vectors $\mathbf{a}_n(z)$ depend on the transversal coordinate z , being spatial modal eigenforms in the plate's cross-section; ζ_n are wavenumbers; ω is the angular frequency of

steady-state time harmonic oscillation $e^{-i\omega t}$; t_n are factors determined by the wave source or scatterer (e.g., by the actuating force or reflection coefficients). The dispersion dependencies $\zeta_n = \zeta_n(\omega)$ are obtained as roots of certain transcendent characteristic equations $\Delta(\zeta, \omega) = 0$ which can be explicitly written in a closed form. Being numerically obtained, the roots ζ_n yield the Lamb mode phase and group velocities $v_{p,n} = \omega/\zeta_n$ and $v_{g,n} = d\omega/d\zeta_n$, used, for instance, for TOF estimation.

However, in the 3D case, the wave fields are represented via two-fold path integrals, and the residue technique cannot bring them to explicit analytical expressions. As a compromise decision, it was proposed that one of these two-fold integrations be evaluated analytically, using the residue technique, while the remaining one be performed numerically [2]. As an alternative to numerical integration, an approximation of a 3D GW radiation in an anisotropic plate by a superposition of 2D plane waves has been also implemented [25].

At the same time, similar to Eq. (1) closed representations for cylindrical GWs, strictly accounting for the actuating force and the directivity induced by anisotropy, had been already derived in the course of our activities in this field that goes back to the 1980s. Unfortunately, at that time it was not properly published and its description was only available in internal reports and papers in Russian. Due to the increasing interest in composite materials, more implementations of this approach have been accomplished in last years, and its summary description in English has appeared at last [7, 10].

The objective of the present paper is to demonstrate the abilities of these representations by two examples of specific theoretical and experimental research. First, this is a reconstruction of effective material constants of a fiber-reinforced composite plate, which is based on the data acquired by means of laser Doppler vibrometry (LDV) of PWAS actuated surface waves (Section 4). Then an example of experimentally confirmed central frequency tuning, performed with accounting for radiation directivity caused by fibers, is given in Section 5. Previously, Section 2 provides a summary of the mathematical framework, which is illustrated by numerical examples, while the experimental setup is specified in Section 3.

It is worthy to note that all experimental measurements included in the paper have been carried out in the headed by Prof. R. Lammering Institute of Mechanics, Helmut-Schmidt-University, Hamburg, using its excellent equipment facilities.

2 Theoretical background

A more detailed description of the mathematical framework used for computer simulation may be found in Ref. [7] and papers cited therein. The present section gives just a brief review of the approach and the final GW representations used in the computations, keeping the notations of paper [7].

Mathematically, the elastodynamic response $\mathbf{u}(\mathbf{x}, \omega)e^{-i\omega t}$ of a laminate composite plate to a steady-state time-harmonic loading $\mathbf{q}(x, y)e^{-i\omega t}$ applied to a finite area Ω on its top surface (Fig. 1) is described by a solution of a boundary value problem with respect to the complex amplitude of the displacement vector $\mathbf{u} = (u_x, u_y, u_z) = (u_1, u_2, u_3)$. In Cartesian coordinates $\mathbf{x} = (x, y, z) = (x_1, x_2, x_3)$ the structure occupies the layer domain $D = \cup_{m=1}^M D_m$: $|x| < \infty, |y| < \infty, -H \leq z \leq 0$, composed of the sublayers

$$D_m : |x| < \infty, |y| < \infty, z_{m+1} \leq z \leq z_m, \quad m = 1, 2, \dots, M$$

with different material properties. Here $z_1 = 0, z_{M+1} = -H, H = \sum_{m=1}^M h_m$ is the thickness of the whole structure and $h_m = z_m - z_{m+1}$ are the thicknesses of sublayers; $\omega = 2\pi f$ is the angular frequency, f is the frequency. Below the harmonic factor $e^{-i\omega t}$ is omitted. In

every sublayer the displacement components u_i obey the elastodynamic equations in displacements

$$C_{ijkl}u_{l,jk} + \rho \omega^2 u_i = 0, \quad i = 1, 2, 3. \quad (2)$$

The elastic stiffness tensor C_{ijkl} and the density ρ keep constant values within every sublayer D_m , thus, they are piecewise constant functions of the transverse coordinate z . It is assumed that the outer sides of the waveguide $z = 0$ and $z = -H$ are stress-free except the loading area Ω , and the sublayers are perfectly bonded.

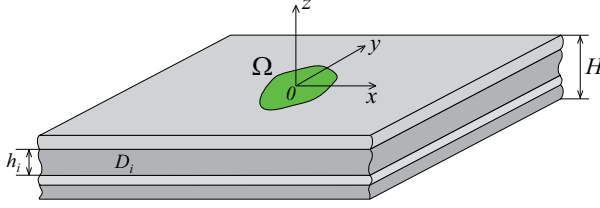


Fig. 1 Geometry of problem.

In the general case, the applied load \mathbf{q} may be of different nature. In particular, it may describe distribution of contact stresses under an interacting body (indenter, transducer, piezopatch actuator, and so on) or simulate the effect of laser-generated thermal stresses. Using the Fourier transform \mathcal{F}_{xy} with respect to the horizontal coordinates x and y , applied to Eq. (2) and to the boundary conditions at the plate sides and interfaces $z = z_m$, the structure's response $\mathbf{u}(\mathbf{x}, \omega)$ can be represented via the convolution of the structure's Green's matrix $k(\mathbf{x}, \omega)$ with the load vector-function \mathbf{q} :

$$\mathbf{u} = k * \mathbf{q} = \iint_{\Omega} k(x - \xi, y - \eta, z) \mathbf{q}(\xi, \eta) d\xi d\eta \quad (3)$$

or, alternatively, via their Fourier symbols $K = \mathcal{F}_{xy}[k]$ and $\mathbf{Q} = \mathcal{F}_{xy}[\mathbf{q}]$:

$$\mathbf{u}(\mathbf{x}) = \mathcal{F}_{xy}^{-1}[K\mathbf{Q}] = \frac{1}{4\pi^2} \int_{\Gamma^+} \int_0^{2\pi} K(\alpha, \gamma, z) \mathbf{Q}(\alpha, \gamma) e^{-i\alpha r \cos(\gamma - \varphi)} d\gamma d\alpha. \quad (4)$$

The columns \mathbf{k}_j of the Green's matrix k are the displacement vectors excited by concentrated point loads applied to the surface $z = 0$ along the basic vectors \mathbf{i}_j , $j = 1, 2, 3$. In Eq. (4) the Cartesian variables \mathbf{x} and the Fourier parameters $\alpha = (\alpha_1, \alpha_2)$ are taken in the cylindrical and polar coordinates (r, φ, z) and (α, γ) , respectively. Integration contour Γ^+ goes in the complex plane α along the real semi-axis $\text{Re}\alpha \geq 0$, $\text{Im}\alpha = 0$, bypassing real poles $\zeta_n = \zeta_n(\gamma) > 0$ of the matrix K elements according to the principle of limiting absorption.

Efficient computer implementation of these explicit solutions is based on the fast and reliable algorithms of Green's matrix calculation. With a given \mathbf{Q} (either in a closed analytical form or approximately, e.g. via a contact problem solution [9], or a FEM simulation [3]), the response \mathbf{u} inside the area Ω and in a not distant vicinity can be obtained via direct numerical integration of integral (4), while with increasing distance r , the computational expenses also increase due to the oscillating factor $\exp(-i\alpha r \cos(\gamma - \varphi))$ in the integrand. In the 2D case,

when the integrals for \mathbf{u} are one-dimensional, this restriction is conventionally overcome by the use of the residue technique yielding plane GWs of form (1) as the residues from the poles ζ_n . With isotropic materials and axially symmetric loadings (including with the point loads yielding Green's matrix k), the integration over γ in Eq. (4) can be performed analytically, so that the two-fold inverse Fourier integrals are reduced to one-dimensional path integrals of inverse Fourier-Bessel transform. The residue technique is also applicable to such integrals leading to explicit representations of cylindrical GWs in terms of cylindrical Hankel functions.

The anisotropy of elastic properties usually makes analytical integration impossible even for the matrix $k(\mathbf{x})$ components. Therefore, the derivation of GW asymptotics from Eq. (4) is obtained via the application the residue theorem to the integral over path Γ^+ in combination with the stationary phase method for remaining integral over γ . It brings the explicit integral representation for Green's matrix k to the asymptotic expansion [7]

$$\begin{aligned}
k(\mathbf{x}) &= \sum_{n=1}^{N_r} k_n(\mathbf{x}) + O((\zeta r)^{-1}) \quad r \rightarrow \infty \\
k_n(\mathbf{x}) &= \sum_{m=1}^{M_n} b_{nm}(\varphi, z) e^{is_{nm}r} / \sqrt{\zeta_n r} [1 + O((\zeta_n r)^{-1})], \quad r \rightarrow \infty \\
b_{nm} &= \sqrt{2i\zeta_n / (\pi s_n''(\gamma_m))} R_n(\theta_m, z), \\
R_n(\theta_m, z) &= \frac{i}{2} \zeta_n \text{res} K(\alpha, \theta_m, z) |_{\alpha=\zeta_n} \\
s_{nm} &= s_n(\gamma_m) = \zeta_n(\theta_m) \sin \gamma_m, \quad \theta_m = \gamma_m + \varphi + \pi/2,
\end{aligned} \tag{5}$$

where γ_m are stationary points of the oscillating exponentials (the roots of the equation $s_n'(\gamma) = 0$), M_n is the number of roots γ_m in the interval $0 < \gamma < \pi$, N_r is the number of real poles ζ_n .

To obtain a far-field asymptotic representation for GWs generated by a load \mathbf{q} , it is enough to substitute expansion (5) into convolution (3) and to implement a cubature discretization over Ω :

$$\begin{aligned}
\mathbf{u}(\mathbf{x}) &= \sum_{n=1}^{N_r} \mathbf{u}_n(\mathbf{x}) + O((\zeta r)^{-1}), \quad \zeta r \rightarrow \infty \\
\mathbf{u}_n(\mathbf{x}) &= h^2 \sum_{j=1}^{N_j} \sum_{m=1}^{M_{nj}} b_{nm}(\varphi_j, z) \mathbf{q}_j e^{is_{nmj}r_j} / \sqrt{\zeta_n r_j}.
\end{aligned} \tag{6}$$

Here $\mathbf{q}_j = \mathbf{q}(x_j, y_j)$, (x_j, y_j) are cubature nodes covering Ω with a spacing h ; $r_j = \sqrt{(x-x_j)^2 + (y-y_j)^2}$ and $\varphi_j : \cos \varphi_j = (x-x_j)/r_j$, $\sin \varphi_j = (y-y_j)/r_j$; the stationary phase equations have to be solved for every direction φ_j , M_{nj} is a number of roots γ_{mj} for $\varphi = \varphi_j$; $s_{nmj} = s_n(\gamma_{mj})$.

Every terms of the second sum in Eq. (6) is nothing else than a cylindrical GW propagating from the elementary source $h^2 \mathbf{q}_j \delta(x-x_j, y-y_j)$ with phase and group velocities ω/s_{nmj} and $(ds_{nmj}/d\omega)^{-1}$. Their wavenumbers $s_{nmj} = \zeta(\theta_{mj}) \sin \gamma_{mj}$ depend on the direction of propagation φ , while with an isotropic sample $\gamma_{mj} = \pi/2$, and they degenerate into the independent of φ poles ζ_n . Thus, the terms \mathbf{u}_n are superpositions of guided waves generated by elementary sources located at the nodes $\mathbf{x}_j = (x_j, y_j, 0)$. They propagate with velocities which are approximately equal to those associated with the direction φ . At large enough distances, when all the directions φ_j become practically parallel to each other ($\varphi_j \approx \varphi$), one

can obtain the more compact asymptotic representation

$$\mathbf{u}_n(\mathbf{x}) \sim \sum_{m=1}^{M_n} \mathbf{a}_{nm}(\varphi, z) e^{i s_{nm} r} / \sqrt{\zeta_n r}, \quad \zeta_n r \rightarrow \infty \quad (7)$$

$$\mathbf{a}_{nm} = b_{nm}(\varphi, z) \mathbf{Q}(-s_{nm}, \varphi)$$

which is valid for relatively large distances in comparison with the size of Ω . These representation is especially convenient when a close analytical form of $\mathbf{Q}(\alpha, \gamma)$ is available.

The amplitude functions $\mathbf{a}_{nm}(\varphi, z)$ coincide to constant factors with the GW modal eigenforms that may be derived using conventional modal analysis technique. The series expansions (6) and (7) provide a computationally efficient and physically clear analytically-based tool for GW analysis, which already accounts for the source influence on the host structure through the vector-functions $\mathbf{q}(x, y)$ or $\mathbf{Q}(\alpha, \gamma)$.

Transient wave fields $\mathbf{u}(\mathbf{x}, t)$ generated by non-harmonic loads can be obtained via the frequency spectrum $\mathbf{u}(\mathbf{x}, \omega)$ using fast Fourier transform (FFT) or B-spline approximate integration in the frequency domain.

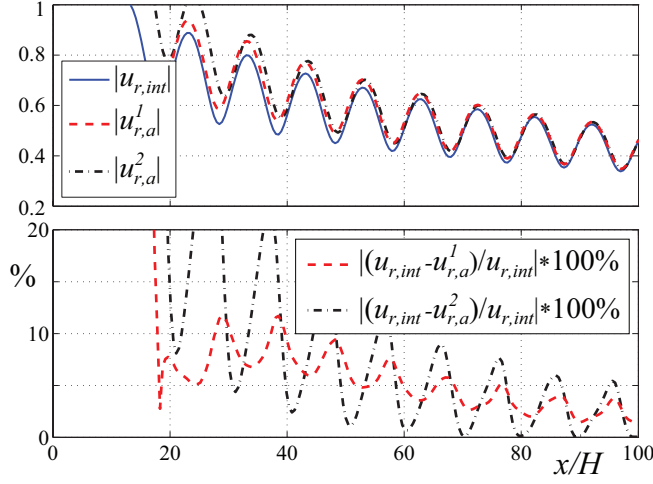


Fig. 2 Radial displacements $|u_r(x, 0, 0)|$ versus the distance x/H from actuator calculated via numerical integration (4) and using asymptotics (6) and (7).

To illustrate the applicability of expressions (6) and (7), let us consider a time-harmonic oscillation of a transversally isotropic layer of the thickness $H = 1$ mm with fibers oriented along the x axis, the elastic properties taken from paper [28]: $C_{11} = 130.7$, $C_{12} = 5.2$, $C_{22} = 13.0$, $C_{23} = 4.5$, $C_{55} = 6.0$ (GPa), and $\rho = 1578$ kg/m³. The elastic constants are given here in the conventional two-index Voigt notation. A ring delta-like distribution of a surface radial tension τ_r serves as a surface load:

$$\mathbf{q} = \tau_r (\delta_r(r - a) \cos \varphi, \delta_r(r - a) \sin \varphi). \quad (8)$$

The latter is proved to be a suitable approximation of thin piezopatch action on a plate structure in the frequency range below 500 kHz-mm [5, 20]. Figures 2(a) and 3(a) display

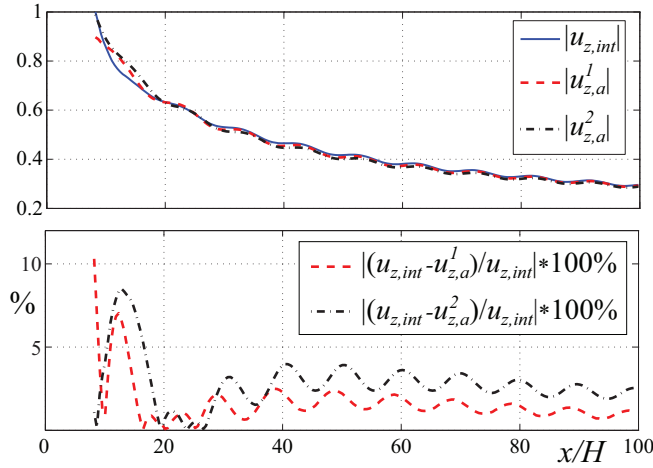


Fig. 3 Out-of-plane displacements $|u_z(x,0,0)|$ versus the distance x/H from actuator calculated via numerical integration (4) and using asymptotics (6) and (7).

the plots of normalized radial and out-of-plane amplitudes $|u_r|$ and $|u_z|$ versus the distance x/H from the center of the ring source (8) with a radius of $a = 8$ mm at a frequency of $f = 10^3/(2\pi)$ kHz, the s_0 and a_0 wavelengths are $\lambda_s = 57.0$ mm and $\lambda_a = 8.3$ mm, respectively. The calculations were performed using Eq. (4) ($|u_{r,int}|$ and $|u_{z,int}|$, solid lines), Eq. (6) ($|u_{r,a}^1|$ and $|u_{z,a}^1|$, dashed lines, points (x_j, y_j) are evenly spaced along the ring) and Eq. (7) ($|u_{r,a}^2|$ and $|u_{z,a}^2|$, dashed-dotted lines). It should be noted that in this example, the symmetric mode s_0 predominates in the radial displacements, while the antisymmetric mode a_0 - in the out-of-plane ones. Additionally, relative discrepancy (in percents) between the integral and asymptotic values are given in the bottom subplots. One can see a good agreement of the results which become better as the distance x/H increases, going down beneath the 3% level for $x/H > 2\lambda$ of the corresponding mode. It is sufficient to mention that in the case considered, the evaluation of $|u_{int}|$ in 250 points along the x axis takes about 12 minutes at an ordinary laptop equipped with Intel Core i330M CPU. At the same time, the calculation of $|u_a^1|$ requires 1 minute, while only 5 seconds are quite enough for $|u_a^2|$.

3 Experimental setup

For experimental verification of the computer models developed, a carbon-fiber-reinforced polymer (CFRP) plate manufactured by Carbotec GmbH with the lay-up $[0^\circ]_4$ and the dimensions $1000 \times 1000 \times 1.1$ mm³ have been used. Elastic properties of the plate except the density $\rho = 1482$ kg/m³ were initially unknown and thus had to be estimated beforehand.

The plate is driven by a circular vertically polarized piezoceramic actuator (provided by PI Ceramic GmbH, PIC151 ceramic) glued to its surface (radius of the electroded area $a = 7.8$ mm, thickness $b = 0.25$ mm). The velocity field of propagating waves is measured by means of a Polytec PSV-400 scanning laser vibrometer coupled with a Tektronix TDS 1012B two-channel digital storage oscilloscope. The scanning head of the PSV-400 system is placed 1.32 m above the specimen. A thin reflective film is glued to the surface of the

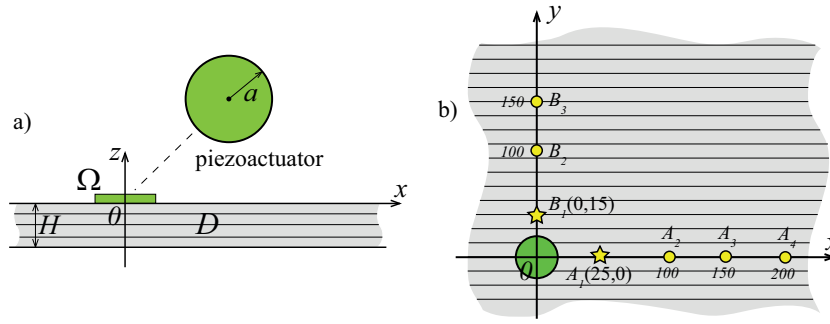


Fig. 4 Sketch of the experimental setup: (a) side view and (b) top view

plate in the area of observation, which is proved to be a suitable tool for improving the laser beam reflection and minimizing the signal-to-noise ratio.

In the frequency range below 160 kHz-mm the actuator is excited by a sine windowed two-cycle sine tone-burst, which at higher frequencies is changed by a five-cycle Hann windowed sine signal in order to provide a narrower frequency support. For this purpose a Tektronix AFG 3022B two-channel arbitrary signal generator is used. The generated signal is 100 times amplified (Develovic WBHV 2A600 amplifier) to reach the amplitude $145 V_{pp}$ before it is applied to the actuator. To obtain the frequency response in various propagation directions the actuator is driven by a periodic chirp generated by the vibrometer hardware and covering the range from 10 kHz to 350 kHz. The FFT is then applied to the measured signals. The sketch of the plate used in the experiments is given in Fig. 4.

4 Reconstruction of material properties

There exist various techniques for measuring elastic properties of composite materials. Conventional approaches like tensile, compressive and shear tests are destructive in nature and non-capable to reconstruct all the elastic moduli. Vibration-based and ultrasonic approaches are more advantageous over the conventional techniques due to their nondestructive manner and a possibility to estimate several moduli simultaneously. Experimentally obtained vibration eigenfrequencies are used for the prediction of composite mechanical properties [15], while the ultrasonic techniques utilize either elastic bulk waves or guided Lamb waves.

It was shown that ultrasonic bulk wave velocities are insensitive to a variation of some material constants [26] and, consequently, not all of the elastic moduli can be reconstructed using the bulk waves. Another limitation, typical for both bulk wave and vibration-based methods, is that they require specially prepared samples, whereas the Lamb wave based methods may be directly implemented to the engineering structure under investigation.

Based on the mathematical model described above, an algorithm for the determination of effective elastic constants of fiber-reinforced plates has been developed and applied to the plate under study. This algorithm is close to that described in papers [21, 27]. It consists in the minimization of discrepancy between the theoretically calculated and experimentally measured dispersion curves in the course of constants C_{ij} variation. Unlike to the cited works, where phase velocities were used, the group velocities of fundamental antisymmetric (a_0) and symmetric (s_0) Lamb waves measured along the symmetry axes of the composite at varying excitation frequencies serve as a data input to the inverse identification. In addition,

of course, it differs by the use of analytically-based tools described above for the objective function calculation. The plate is modeled as a single transversally isotropic layer with fibers oriented along the x axis, so that 5 independent effective elastic moduli are to be estimated, namely, C_{11} , C_{12} , C_{22} , C_{44} and C_{55} .

The algorithm consists of the following steps:

1. Guided waves are generated via the piezoactuator excited by the windowed tone-bursts of varying central frequencies. The out-of-plane velocities $v_z(x, y, 0, t)$ are measured with the laser vibrometer along the fiber orientation direction (points $A_2(100, 0)$, $A_3(150, 0)$ and $A_4(200, 0)$, Fig. 3(b)) and in the perpendicular one (points $B_2(0, 100)$ and $B_3(0, 150)$). These directions have been utilized for measurements due to sensitivity reasons, e.g., in the frequency range of interest, the velocities of a_0 and s_0 modes along the x axis depend mainly on C_{11} and C_{55} moduli, while the parameters C_{22} and C_{44} are responsible for the perpendicular direction [13].
2. In order to extract group velocities from the obtained transient signals, they are processed with the Gabor wavelet transform. It has been shown that the arrival times of wave packages at each local frequency can be extracted by using the magnitude peaks of the wavelet coefficients [12]. The a_0 and s_0 group velocities are received by dividing the propagation lengths (the distances between the center of actuator and the measurement points) by the corresponding arrival times. The obtained values are then averaged along the specific direction.

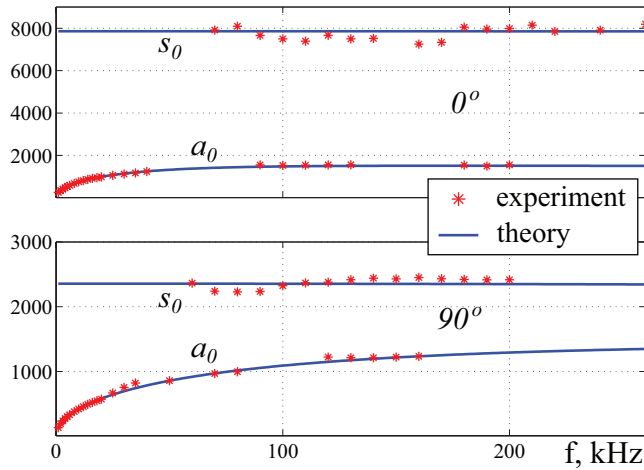


Fig. 5 Measured and theoretically calculated with the restored elastic constants group velocity dispersion curves (in m/s) for a_0 and s_0 modes along the fibers (upper plot) and in the perpendicular direction (bottom plot).

3. At the next step, the objective function is constructed in the form

$$ERR(C) = \sum_{j=1}^N \alpha_j^2 (v_{g,j}^m - v_{g,j}^c)^2, \quad (9)$$

where C is a candidate matrix of material constants C_{ij} constrained by some initially prescribed boundary values: $C_{min} \leq C \leq C_{max}$, v_g^m and v_g^c are measured and computed group

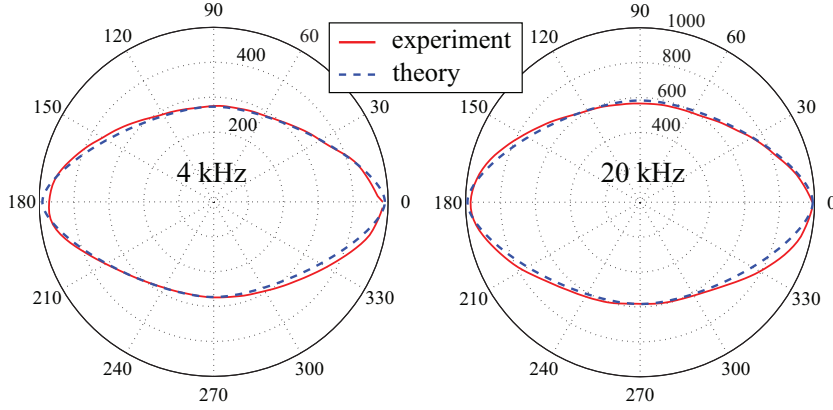


Fig. 6 Measured and theoretically restored angular dependences of the a_0 group velocity for $f = 4$ kHz and $f = 20$ kHz.

velocities, N is the total amount of measured velocities (both for a_0 and s_0 modes); $a_j = v_{max}/v_{g,j}^m$ are normalizing coefficients, $v_{max} = \max(v_{g,j}^m)$, $j = 1, 2, \dots, N$. To calculate the values of v_g^c , the first real poles $\zeta_n(\gamma)$, $n = 1, 2, \dots, N_r$ of the Green's matrix Fourier symbol $K(\alpha, \gamma)$ are traced using dichotomy technique and refined with Muller's method. After that, the group velocity vector is calculated using the formula [28]:

$$\mathbf{v}_g = \begin{pmatrix} v_{gx} \\ v_{gy} \end{pmatrix} = \begin{bmatrix} \cos \gamma & -\sin \gamma \\ \sin \gamma & \cos \gamma \end{bmatrix} \begin{pmatrix} \partial W / \partial \alpha \\ \frac{\partial W}{\alpha \partial \gamma} \end{pmatrix},$$

in which $\omega = W(\alpha, \gamma)$ is the dispersion equation derived in terms of matrix $K(\alpha, \gamma, z)$ elements.

4. Since objective (9) is a sum of the least-square errors between the measured and calculated data, it has to be minimized. For this purpose a real coded micro-genetic algorithm (μ GA) [14] with a simulated binary crossover [4] is applied. Every individual chromosome represents a candidate solution (matrix C). Thus the sum $ERR(C)$ is its fitness value.

After numerical testing of this algorithm on a composite with initially known properties, it has been applied to the investigated specimen and the following approximate values for the elastic moduli have been obtained (in GPa):

$$C_{11} = 95.93, \quad C_{12} = 3.57, \quad C_{22} = 9.61, \quad C_{44} = 3.0, \quad C_{55} = 3.3.$$

or in terms of engineering constants:

$$E_1 = 94.0 \text{ GPa}, \quad E_2 = 8.2 \text{ GPa}, \quad \mu_{12} = 0.27, \quad G_{23} = 3.0 \text{ GPa}, \quad G_{12} = 3.3 \text{ GPa}$$

Figure 5 depicts measured and theoretically restored group velocities of a_0 and s_0 modes versus frequency for both x and y directions. Figure 6 shows angular dependencies of a_0 group velocity at the two frequencies $f = 4$ kHz and $f = 20$ kHz, while Figure 7 depicts calculated and measured a_0 wavelengths along the x and y axes versus frequency. A conventional approach based on two-dimensional time-spatial Fourier transform [1] has been utilized for obtaining the experimental wavelengths. In all the cases a good coincidence with the total error less than 5% is obtained.

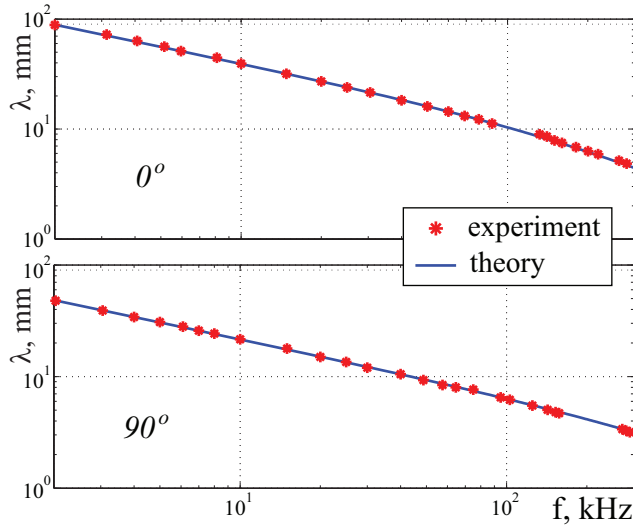


Fig. 7 Measured and theoretically restored a_0 mode wavelength dispersion curve (in mm) along the fibers (upper plot) and in the perpendicular direction (bottom plot). The axes are in a logarithmic scale.

Moreover, to verify the obtained results, destructive tensile tests have also been performed by M.-N. Neumann (Institute of Mechanics, Helmut-Schmidt-University, Hamburg). The following values of Young moduli have been obtained: $E_{1,t} = 105.7$ GPa and $E_{2,t} = 7.5$ GPa. These values are in a good qualitative agreement with the restored effective elastic moduli above. A slight quantitative difference in the direction along the fibres may be explained by a certain inaccuracy in the s_0 group velocity LDV measurement due to a relatively small out-of-plane amplitude of this mode.

5 Radiation directivity and frequency tuning

Theoretical and experimental investigations of unidirectional and cross-ply laminates driven by circular piezoelectric actuators [7, 17] have shown that unlike to the point source case, the main radiation lobe periodically alternates either along the upper-ply fibers or in the perpendicular direction in the course of frequency or source diameter variation. The alternation takes place only with sized source. It can be theoretically explained through the in-phase or out-of-phase interaction of wave packages generated by the opposite actuator's edges. Therefore, due to the angular variation of the GW wavelengths caused by the material anisotropy, the so-called tuning frequencies [6] become also angle dependent. At such frequencies a piezosensor registers a maximum amplitude ratio between the s_0 and a_0 modes. With a 1D laser vibrometry, these frequencies are equal or close to those where the a_0 mode has local peaks.

To understand the influence of material anisotropy on the GW directivity, the points A_1 and B_1 (Fig. 3) in the directions along and across the fibers have been selected for the frequency response measurement and simulation. The plots of the normalized out-of-plane velocity magnitude $|v_z| = \omega|u_z|$ measured and computed at these points are shown in Fig. 6. The theoretical results depicted by the dashed lines are obtained using Eq. (6). One can see

a good agreement of the predicted and measured optimal frequencies. The curves exhibit alternations of minima and maxima typical for dimensional sources [6, 8]. In distinction to the isotropic case, the frequencies of local minima and maxima of these curves do not generally coincide due to the difference in modal wavelengths along and across the fibers. Correspondingly, the optimal central excitation frequencies f_c varies with propagation directions.

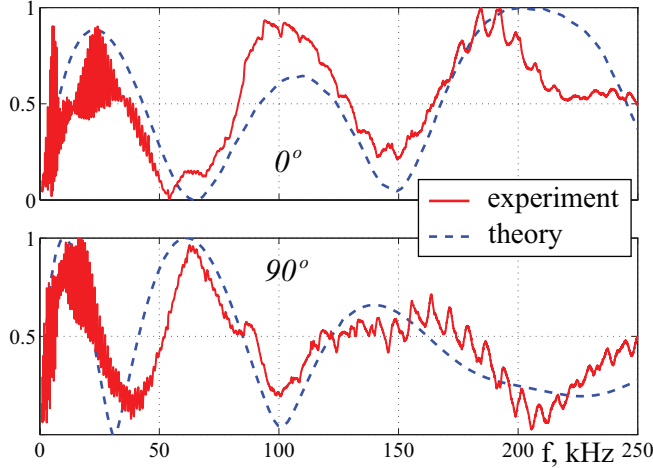


Fig. 8 Frequency spectrum of the out-of-plane velocity amplitudes $|v_z|$ at the points A_1 (top) and B_1 (bottom); experimental measurements (solid line) and theoretical simulation (dashed line). The upper plot refers to the direction along fibers, the bottom plot is for the perpendicular one.

To illustrate how a proper choice of f_c influences on the wave propagation patterns, the experimental and predicted transient out-of-plane normalized velocities $v_z(x, t)$ at the points A_2 and B_2 are added in Fig. 7. In the subplots (a) and (b) the actuator is driven with a sine windowed two-cycle sine tone-burst, while (c) and (d) subplots show results of a five-cycle Hann windowed sine signal. The viscosity is implicitly taken into account in Eq. (6) or (7) by introducing new exponents $s_{nm}^* = s_{nm} - ib\omega$, where b is a small real constant different for the directions along and perpendicular to the fibers ($b = 0.01 - 0.02$ and $b = 0.04 - 0.06$, respectively); here $s_{nm} := s_{nm} * H$ and $\omega = 2 * \pi * f * H / c_T$ are dimensionless parameters used in calculations, $c_T = 1000$ m/s is a unit of velocity.

As it was expected [8], the a_0 wave packages excited at the frequencies where local maxima of $|v_z|$ occur (subplots (b) and (c)) propagate without visible dispersion. On the contrary, in two other cases the contribution of the central frequency f_c is suppressed and the frequency spectrum is actually broken down into two independent parts with new central frequencies on each side of f_c . As the result, the wave packages in subplots (a) and (d) become blurred, tending to split into two separate packages propagating with different group velocities. At these frequencies and directions, the dispersion curves are poorly restored from experimental data. It should be also noted that in the low-frequency range the maximum in one of the directions occur almost at the minimum of the counterpart one. Thus, selecting, for example, the frequency $f_c = 65$ kHz as a global optimum for the whole plate monitoring, one can acquire signals of poor quality in the fiber direction.

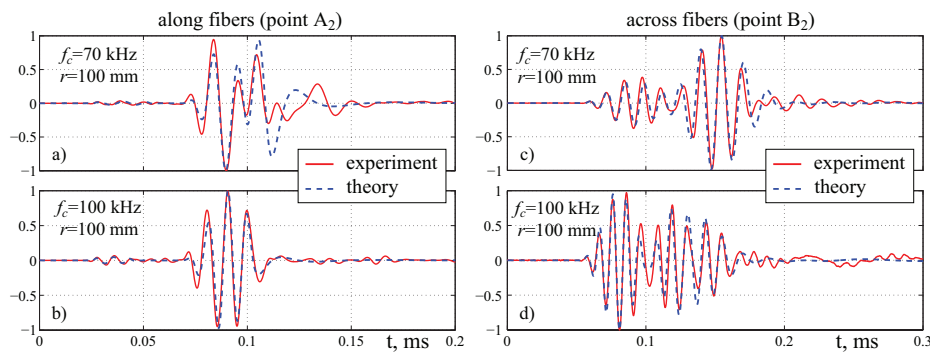


Fig. 9 Influence of propagation directions and central excitation frequencies on the transient normalized out-of-plane velocities $v_z(x, t)$ recorded and calculated at the points A_2 and B_2 .

6 Conclusion

The experimentally validated integral and asymptotic representations derived based on the Green's matrix concept have been proved to be an efficient tool for low-cost computer modeling of forced wave dynamics of laminate anisotropic composite structures, in particular, in the interests of ultrasonic guided wave structural health monitoring.

Acknowledgements The authors are grateful to Prof. R. Lammering, Helmut Schmidt University, Hamburg, for the fruitful cooperation. The work is partly supported by the Russian Foundation for Basic Research (pr. No. 12-01-00320 and 12-01-33011), Russian Ministry for Education and Science (pr. No. 10.61.2011), and Deutscher Akademischer Austauschdienst (DAAD).

References

1. Alleyne, D., Cawley, P.: A two-dimensional fourier transform method for the measurement of propagating multimode signals. *Journal of the Acoustical Society of America* **89**(3), 1159–1168 (1991)
2. Banerjee, S., Prosser, W., Mal, A.: Calculation of the response of a composite plate to localized dynamic surface loads using a new wave number integral method. *Journal of Applied Mechanics* **72**(1), 18–24 (2005)
3. Collet, M., Ruzzene, M., Cunefare, K.A.: Generation of lamb waves through surface mounted macro-fiber composite transducers. *Smart Materials and Structures* **20**(2), 025,020 (2011)
4. Deb, K., Agrawal, R.B.: Simulated binary crossover for continuous search space. *Complex Systems* **9**(2), 115–148 (1995)
5. Ende, S.v., Lammering, R.: Investigation on piezoelectrically induced Lamb wave generation and propagation. *Smart Mater. Struct.* **16**, 1802–1809 (2007)
6. Giurgiutiu, V.: *Structural health monitoring - with piezoelectric wafer active sensors*. Academic Press, Amsterdam, Boston (2008)
7. Glushkov, E., Glushkova, N., Eremin, A.: Forced wave propagation and energy distribution in anisotropic laminate composites. *Journal of the Acoustical Society of America* **129**(5), 2923–2934 (2011)
8. Glushkov, E., Glushkova, N., Lammering, R., Eremin, A., Neumann, M.N.: Lamb wave excitation and propagation in elastic plates with surface obstacles: proper choice of central frequencies. *Smart Materials and Structures* **20**(1), 015,020 (2011)
9. Glushkov, E.V., Glushkova, N.V., Kvasha, O.V., Seemann, W.: Integral equation based modeling of the interaction between piezoelectric patch actuators and an elastic substrate. *Smart Materials and Structures* **16**(3), 650664 (2007)
10. Glushkov, Y., Glushkova, N., Krivonos, A.: The excitation and propagation of elastic waves in multilayered anisotropic composites. *Journal of Applied Mathematics and Mechanics* **74**(3), 297 – 305 (2010)

11. Gopalakrishnan, S., Chakraborty, A., Roy Mahapatra, D.: Spectral Finite Element Method: Wave Propagation, Diagnostics and Control in Anisotropic and Inhomogeneous Structures. Springer London (2008)
12. Kishimoto, K., Inoue, H., Hamada, M., Shibuya, T.: Time Frequency Analysis of Dispersive Waves by Means of Wavelet Transform. *Journal of Applied Mechanics* **62**(4), 841–846 (1995)
13. Lasn, K., Klauson, A., Chati, F., Dcultot, D.: Experimental determination of elastic constants of an orthotropic composite plate by using lamb waves. *Mechanics of Composite Materials* **47**, 435–446 (2011)
14. Liu, G., Ma, W., Han, X.: An inverse procedure for determination of material constants of composite laminates using elastic waves. *Computer Methods in Applied Mechanics and Engineering* **191**(33), 3543 – 3554 (2002)
15. Maletta, C., Pagnotta, L.: On the determination of mechanical properties of composite laminates using genetic algorithms. *International Journal of Mechanics and Materials in Design* **1**, 199–211 (2004)
16. Nadella, K., Cesnik, C.: Local interaction simulation of guided-wave propagation in composite plates. *Proc. SPIE* **7984**, 79,841X–79,841X–9 (2011)
17. Nadella, K.S., Salas, K.I., Cesnik, C.E.S.: Characterization of guided-wave propagation in composite plates. In: Society of Photo-Optical Instrumentation Engineers (SPIE) Conference Series, *Society of Photo-Optical Instrumentation Engineers (SPIE) Conference Series*, vol. 7650 (2010)
18. Nayfeh, A.H.: The general problem of elastic wave propagation in multilayered anisotropic media. *The Journal of the Acoustical Society of America* **89**(4), 1521–1531 (1991)
19. Ostachowicz, W., Kudela, P., Krawczuk, M., Zak, A.: Spectral Finite Element Method, in *Guided Waves in Structures for SHM: The Time-Domain Spectral Element Method*. John Wiley & Sons, Ltd (2012)
20. Raghavan, A., Cesnik, C.E.S.: Finite-dimensional piezoelectric transducer modeling for guided wave based structural health monitoring. *Smart Materials and Structures* **14**(6), 1448 (2005)
21. Rogers, W.P.: Elastic property measurement using rayleigh-lamb waves. *Research in Nondestructive Evaluation* **6**, 185–208 (1995)
22. Rokhlin, S., Wang, L.: Ultrasonic waves in layered anisotropic media: characterization of multidirectional composites. *International Journal of Solids and Structures* **39**(16), 4133 – 4149 (2002)
23. Rose, J.L.: *Ultrasonic Waves in Solid Media*. Cambridge University Press, Cambridge, UK (1999)
24. Schulte, R.T., Fritzen, C.P., Moll, J.: Spectral element modelling of wave propagation in isotropic and anisotropic shell-structures including different types of damage. *IOP Conference Series: Materials Science and Engineering* **10**(012065), 1–10 (2010)
25. Velichko, A., Wilcox, P.D.: Modeling the excitation of guided waves in generally anisotropic multilayered media. *Journal of the Acoustical Society of America* **121**(1), 60–69 (2007)
26. Vishnuvardhan, J., Krishnamurthy, C., Balasubramaniam, K.: Genetic algorithm reconstruction of orthotropic composite plate elastic constants from a single non-symmetric plane ultrasonic velocity data. *Composites Part B: Engineering* **38**(2), 216 – 227 (2007)
27. Vishnuvardhan, J., Krishnamurthy, C.V., Balasubramaniam, K.: Genetic algorithm based reconstruction of the elastic moduli of orthotropic plates using an ultrasonic guided wave single-transmitter-multiple-receiver shm array. *Smart Materials and Structures* **16**(5), 1639 (2007)
28. Wang, L., Yuan, F.: Group velocity and characteristic wave curves of lamb waves in composites: Modeling and experiments. *Composites Science and Technology* **67**(78), 1370 – 1384 (2007)